PREDICTION OF REDUCTION PRODUCTS IN THE PREHEATING PROCESS

by

Guojia YAO, Zuodong LIU, Hong TANG*[*]*, and Lizhi MENG

Northeast Electric Power University, Jilin City, Jilin, China

Original scientific paper
https://doi.org/10.2298/TSCI220919047Y

Under the current requirements of environmental protection, carbon peaking and carbon neutrality goals, the capacity of the new energy interconnection network is increasing day by day. The thermal power unit requires the ability of rapid load adjustment to meet the requirements of real-time power balance. However, when the unit is in a variable load condition, the denitrification system is inefficient or even inoperable. The NO_x emission is large, which makes it difficult to meet environmental protection requirements. In this study, a new method for predicting reductive products in the preheating process is proposed, introducing the gasification mechanism into the pulverized coal preheating process. The effects of air coefficient on combustion temperature, velocity, O_2, CO_2, CO, CH_4, and H_2, volatile matter and NO_x emission are investigated by numerical simulation. It is demonstrated that the gasification mechanism is applicable to predict the reduction products and NO_x during preheating. Internal combustion burners can stabilize the precipitation of volatile matter, CH_4, CO, and H_2. The burner outlet temperature and flow rate decrease with decreasing air coefficient. The local maximum concentration of volatile matter and CH_4 are 8.3 vol.% and 2.54 vol.%, respectively. The CO concentration increases with decreasing air coefficient under the effect of CO_2 gasification reaction. When the air coefficient is 0.33, the NO_x concentration at the burner outlet is 2.8 mg/Nm^3 (at 6% O_2).

Key words*: thermal power unit, pulverized coal preheating, NO_x emission, internal combustion burner, numerical simulation*

Introduction

At present, the concentration of NO_x in economizer inlet and the pressure of denitrification system are high under peak shaving of thermal power units, which could lead to the shutdown of thermal power units. The existing low nitrogen combustion technology combined with denitrification system cannot meet the demand of NO_x emission under variable load conditions. There is an urgent need for a breakthrough low nitrogen combustion technology to reduce the concentration of NO_x at the entrance of the denitrification system.

In recent years, more and more attention has been paid to the pulverized coal preprocessing low nitrogen combustion technology [1-3]. The concrete realization of pulverized coal preprocessing technology [4-7] is to preheat the pulverized coal by a high temperature thermal source before entering the combustion furnace. It makes the pulverized coal release volatile matter quickly and partially burn and gasify to produce a large amount of high tempera-

---

[*] Corresponding author, e-mail: tanghong_neepu@126.com

ture semi-coke. The mixture of high temperature semi-coke and pyrolysis gas is reorganized to achieve low NO_x emission. The preheating process of pulverized coal is shown in fig. 1.

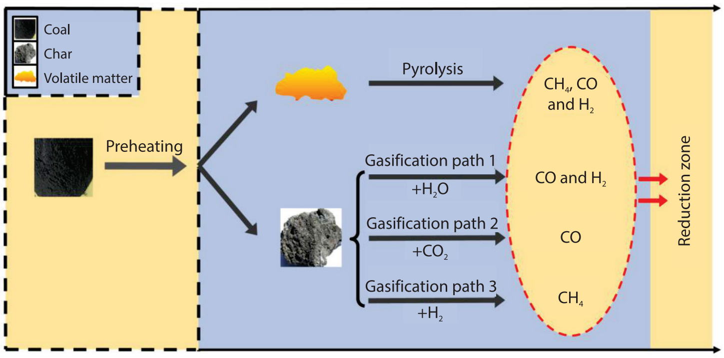

Figure 1. The preheating process of pulverized coal

There are few studies on char gasification during pulverized coal preheating. Most of the simulations related to char combustion have considered only the char oxidation process and ignored the role of gasification [8-11]. This leads to the inability to accurately predict the reduction products. Recently, char gasification at high CO_2 and H_2O concentrations has gained attention. Hecht *et al.* [12] reported that char gasification could increase char conversion and decrease particle temperature. Kim *et al.* [13] found that gasification may lead to a decrease in particle temperature by 200 K, and a similar phenomenon was found by Niu and Shaddix [14]. Many current studies on gasification have focused on high pressure and high concentration gasification conditions [15-17]. The effect of char gasification during the preheating of pulverized coal is not well known.

It is impractical to explore the formation law of pyrolysis products and NO_x only by experiment because of the high operating cost of the experimental equipment. The CFD has been widely used in recent years as an important numerical simulation method for coal combustion guide the design and improvement of actual combustion equipment [18-21]. In this study, the eddy-dissipation concept model assumes that the chemical reactions all occur in small eddy [22-25]. The reaction time is controlled by the combination of the small eddy survival time and the time required for the chemical reaction itself. The model is able to consider detailed gasification reaction mechanisms in turbulent reactions.

The purpose of the study is to accurately predict the generation pattern of reduced products during the preheating of pulverized coal in order to explore the nitrogen reduction potential of preheating technology. Firstly, an internal combustion burner is designed to replace the conventional burner. The measured along-range temperature distribution is used to verify the numerical calculation result under the same boundary conditions. Secondly, the coupled gasification mechanism is used to simulate the pulverized coal preheating process. The calculated temperature is found to have essentially the same trend as the measured temperature by the platinum-rhodium type thermocouple. The generation of reduction products CH_4, H_2, and CO is successfully predicted. Finally, the effects of air coefficients on the temperature, velocity, O_2, CO_2, CO, CH_4, and H_2, volatile matter concentration and NO_x emission in the combustor are investigated. This study provides a scientific basis for predicting the reduction products and nitrogen oxides during the preheating process.

Burner structure and operating conditions

Coal properties

Proximate and ultimate analysis of the coal are shown in tab. 1. Where, *SC* is the abbreviation of Shenhua bituminous coal. The subscript ar represents the coal as received, M_{ar} is the moisture, A_{ar} is the ash, V_{ar} is the volatile matter, FC_{ar} is the fixed carbon, and $Q_{\mathrm{ar,net}}$ is net calorific value of the coal as received.

Table 1. Proximate and ultimate analysis of the coal

	Proximate analysis [%]				Ultimate analysis [%]					$Q_{\mathrm{ar,net}}$ [kJkg^{-1}]
	M_{ar}	A_{ar}	V_{ar}	FC_{ar}	C_{ar}	H_{ar}	O_{ar}	N_{ar}	S_{ar}	
SC	14.50	7.37	28.67	49.46	65.10	3.25	8.08	0.66	0.71	23790

Burner structure and grid

The internal combustion burner adopts a step-by-step amplified ignition structure consisting of a plasma generator, jacket and five-stage internal sleeve [26]. Primary air powder flows out of the burner inlet and a gap between the inner casing layers flows into the inner casing for preheating. The diameter of the burner inlet is 0.59 m, the tail variable square side length is 0.78 m, and the total length is 3.945 m. The wall of the tube is arranged in sequence with five temperature measuring points. The physical and structural diagrams are shown in figs. 2(a) and 2(b). The internal combustion burners replace the original tangential burners. Plasma generator diameter is 0.1 m. The hot plasma enters the primary inner sleeve and immediately ignites the pulverized coal that is carried by the primary air. The heat is sent to the next stage sleeve in turn. Primary air carries most of the pulverized coal from the jacket to the burner. During the flow of pulverized coal, it enters the interior of the burner through the gaps between the internal sleeves and is heated in turn by the heat transferred from the upper sleeve. The graded ignition structure not only forms a stable atmosphere of reduced gas, but also preheats pulverized coal particles evenly. Previous studies have shown that pulverized coal preheating combustion has great potential for reduction of nitrogen emission in the furnace. It is a technology that is expected to meet stringent emission targets through pulverized coal combustion alone.

The number of burner grids is 1050924 cells, all composed of hexahedral structured grids. The burner grid structure is shown in fig. 2(c). The effect of the combustion reaction on the flow field can be better described by grid refinement of the intermediate combustion area.

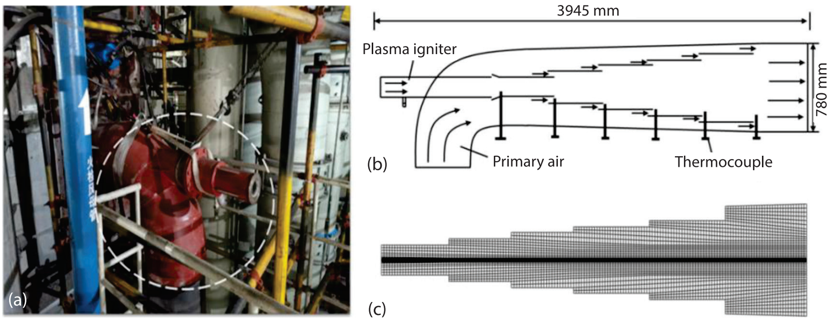

Figure 2. Physical diagram (a), structural diagram (b), and cross-sectional grid diagram (c) of an internal combustion burner

Operating conditions

This study aims to provide experience for the internal combustion burner retrofit of a 600 MW tangentially fired boiler. A total of six cases are simulated as shown in tab. 2 with Shenhua bituminous coal (SC) as the practical coal type for the unit. Case 6 is a full load state and Case 6 is an experimental verification case. Based on the rated working conditions of the power plant burner, the numerical boundary conditions are determined to keep the primary wind speed constant at 22.6 m/s. The plasma is replaced with 3000 K hot air.

Table 2. Numerical simulation case set-up

	Load [ton coal per hour]	Air coefficient
Case 1	5	0.6
Case 2	6	0.5
Case 3	7	0.43
Case 4	8	0.37
Case 5	9	0.33
Case 6	10	0.29

Numerical simulation

Overall model

Numerical simulation is a 3-D gas-solid two-phase flow based on the Euler-Lagrange formulation and performs using commercial code fluent 2020. An Euler framework is used to solve the gas phase conservation equation. The Lagrange framework is used to solve the solid phase equation. An implicit linearized solver based on finite volume pressure is used to couple two interacting source terms. A SIMPLE algorithm is used for pressure-velocity coupling. The spatial derivatives of diffusion terms are discrete by central differential scheme and the stiff non-linear terms are discretized by second order scheme.

Turbulence model is established by the Realizable k-ε model. The stochastic tracking approach is used to describe the motion of discrete coal particles under Lagrange framework. The aerodynamic resistance on dispersed particles is calculated by instantaneous gas velocity. The combustion of coal is simulated as a continuous process of water evaporation, volatilization, char reaction and gas phase combustion. The trajectories of the discrete phase particles are predicted by integrating the forces exerted on the particles without considering the interactions between the particle populations. The interactions between the discrete phase and the continuous phase through mass, momentum, energy and source phase are considered. In the simulation, the continuous phase equation and the discrete phase equation are solved alternately until the solutions of both phases converge [18-20]. The coal particle size is assumed to be consistent with the Rosin-Rammler distribution and divided into 10 discrete sizes with particle diameters 5.8-230 μm. The average particle diameter is 59 μm and the size distribution parameter 1.0 [27, 28]. The particle dispersion due to turbulence in the fluid phase is predicted by a stochastic tracking model. During pulverized coal combustion, radiation is the main energy transfer path in the combustor, transferring more than 90% of the total heat. The discrete ordinate method is used to model the radiation heat transfer. The radiation transfer equation is discretized and solved in the polar and azimuthal directions with an angle of two divisions and four pixels. The gas absorption coefficient is chosen for the WSGGM-domain-based model [29].

Coal devolatilization model

Two-competing model is chosen to describe the pulverized coal devolatilization process. The model can be expressed:

$$\frac{m_\mathrm{v}(t)}{\left(1-f_\mathrm{w,0}\right)m_\mathrm{p,0}-m_\mathrm{a}}=\int_0^t\left(\alpha_1R_1+\alpha_2R_2\right)\exp\left[-\int_0^t\left(R_1+R_2\right)\mathrm{d}t\right]\mathrm{d}t \tag{1}$$

where R_1 and R_2 are the competing kinetic rates for controlled devolatilization in different temperature ranges, $m_\mathrm{v}(t)$ [kg] – the volatile yield at time t, $m_\mathrm{p,0}$ [kg] – the initial particle mass, α_1 and α_2 are 0.3 and 1.0, respectively, m_a [kg] – the ash content in the particle, and $f_\mathrm{w,0}$ – the initial moisture content of the particle.

The two kinetic rates are expressed in the form of Arrhenius:

$$R_1=A_1\exp\left(-\frac{E_1}{\mathrm{R}T_\mathrm{p}}\right),\ R_2=A_2\exp\left(-\frac{E_2}{\mathrm{R}T_\mathrm{p}}\right) \tag{2}$$

where A_1, A_2 and E_1, E_2 [s^{-1} and Jmol^{-1}] are pre-exponential factor and activation energy, the temperature control ranges for R_1 and R_2 are 1000-1700 K and 1700-2100 K, respectively [30], T_P [K] – the pulverized coal particle temperature, and R [$\mathrm{Jmol}^{-1}\mathrm{K}^{-1}$] – the molar gas constant.

In this study, assuming char is composed of pure carbon and ash, the volatile matter is represented by a single pseudo-substance, CaHbOcSdNe, in which a, b, c, d and e are obtained by mass balancing each volatile matter element [31, 32].

Char surface reaction model

Pulverized coal is heated to remove volatile matter in burner. Because of low air coefficient, oxygen consumption is fast and complete and gas phase pressure such as CO_2 increases. Considering that the residual carbon surface will continue to react with gas products (CO_2, H_2, and water vapor) in gas-solid reaction, the multiple surface reactions model is selected to describe char reaction process. The multiple surface reactions model is suitable not only for the oxidation reaction of char, but also for the gasification reaction of char.

Char oxidation reaction:

$$\mathrm{C(s)}+\frac{1}{2}\mathrm{O_2}\rightarrow\mathrm{CO} \tag{R1}$$

$$\mathrm{C(s)}+\mathrm{O_2}\rightarrow\mathrm{CO_2} \tag{R2}$$

Char gasification by water:

$$\mathrm{C(s)}+\mathrm{H_2O}\rightarrow\mathrm{CO}+\mathrm{H_2} \tag{R3}$$

Char gasification by CO_2:

$$\mathrm{C(s)}+\mathrm{CO_2}\rightarrow 2\mathrm{CO} \tag{R4}$$

Char gasification by H_2:

$$\mathrm{C(s)}+2\mathrm{H_2}\rightarrow\mathrm{CH_4} \tag{R5}$$

The char reaction rate is expressed:

$$\overline{R}_{j,r}=A_\mathrm{p}\eta_rY_jR_{k,r} \tag{3}$$

$$R_{j,r}=R_{\mathrm{kin},r}\left(p_\mathrm{n}-\frac{R_{j,r}}{D_{0,r}}\right)^{N_r} \tag{4}$$

where $\bar{R}_{j,r}$ [kg] is the rate of particle surface substance consumption, A_p [m^2] – the particle surface area, Y_j – the mass fraction of substance j in the particle, and η_r – the effectiveness factor related to the surface area of the char. In the process of char consumption, the particle diameter is assumed to remain constant while the density decreases. The $R_{j,r}$ [kgm^{-2}s^{-1}] is the reaction rate of the particle surface substance per unit area, P_n [Pa] – the partial pressure of the gas phase substance, $D_{0,r}$ – the reaction r diffusion rate coefficient, $R_{\mathrm{kin},r}$ – the reaction r kinetic rate, and N_r – the apparent order of the reaction r.

The reaction r diffusion rate coefficients:

$$D_{0,r} = C_{1,r} \frac{\left[\dfrac{T_\mathrm{p} + T_\infty}{2}\right]^{0.75}}{d_\mathrm{p}} \tag{5}$$

where $C_{1,r}$ [kgm^{-3}] is the reaction gas concentration of reaction r, T_p [K] – the particle temperature, T_∞ [K] – the surrounding gas temperature, and d_p [m] – the particle diameter.

The kinetic rate of the reaction r:

$$R_{\mathrm{kin},r} = A_r T_\mathrm{p}^{\beta_r} \mathrm{e}^{-\left(E_r/\mathrm{R}T_\mathrm{p}\right)} \tag{6}$$

When the apparent order of the reaction $N_r = 1$, the rate of consumption of surface material of the particles is given:

$$\bar{R}_\mathrm{j,r} = A_\mathrm{p}\eta_\mathrm{r} Y_\mathrm{j} p_\mathrm{n} \frac{R_\mathrm{kin,r} D_\mathrm{0,r}}{D_\mathrm{0,r} + R_\mathrm{kin,r}} \tag{7}$$

When the apparent order of the reaction $N_r = 0$, the rate of surface material consumption of the particles:

$$\bar{R}_\mathrm{j,r} = A_\mathrm{p}\eta_r Y_j R_{\mathrm{kin},r} \tag{8}$$

Gas-phase reaction model

Despite the great efforts of many researchers, there is no clear, convincing and universally accepted method to define volatiles due to the difficulty of accurately simulating the actual combustion environment and measuring the types of volatiles. In this study, coal volatiles are considered as virtual substances $C_aH_bO_cS_dN_e$. According to the proposal [33], CH_4, CO, and H_2 are considered as the main effective gasses produced by volatile matter pyrolysis. The molar ratio of CH_4 to CO produced by volatile matter pyrolysis is assumed to be 1.59. The equation of volatile matter pyrolysis according to elemental conservation:

$$\mathrm{C}_a\mathrm{H}_b\mathrm{O}_c\mathrm{S}_d\mathrm{N}_e + \frac{2d + 0.39a - c}{2\mathrm{O}_2} \rightarrow 0.61a\mathrm{CH}_4 + 0.39a\mathrm{CO} + \left(\frac{b}{2} - 1.22a\right)\mathrm{H}_2 + d\mathrm{SO}_2 + \frac{e}{2\mathrm{N}_2} \tag{R6}$$

Other homogeneous reactions include water-gas shift reactions:

$$\mathrm{CO} + \mathrm{H_2O} \rightarrow \mathrm{CO_2} + \mathrm{H_2} \tag{R7}$$

$$\mathrm{CO} + \mathrm{H_2} \rightarrow \mathrm{CO} + \mathrm{H_2O} \tag{R8}$$

The CH_4 reforming reaction:

$$\mathrm{CH_4} + \mathrm{H_2O} \rightarrow \mathrm{CO} + 3\mathrm{H_2} \tag{R9}$$

Gas phase products combustion reaction:

$$\mathrm{CO} + \frac{1}{2}\mathrm{O_2} \rightarrow \mathrm{CO_2} \tag{R10}$$

$$\mathrm{CH_4 + 2O_2 \rightarrow CO_{2+} 2H_2O} \tag{R11}$$

$$\mathrm{H_2 + \frac{1}{2} H_2 \rightarrow H_2O} \tag{R12}$$

The kinetic parameters of the aforementioned chemical reactions are shown in tab. 3.

Table 3. Kinetic parameters for chemical reactions

Reaction	A_r [kgs^{-1}m^{-2}atm^{-1}]	E_r [Jkmol^{-1}K^{-1}]	Reference
R1	87100	$1.494 \cdot 10^{08}$	[34, 35]
R2	87100	$1.494 \cdot 10^{08}$	[34, 35]
R3	41800	$1.751 \cdot 10^{08}$	[34]
R4	2470	$1.75 \cdot 10^{08}$	[36]
R5	1.2	$1.49 \cdot 10^{08}$	[36]
R6	1030	100	[32]
R7	$2.34 \cdot 10^{10}$	$2.883 \cdot 10^{08}$	[37]
R8	$2.2 \cdot 10^{07}$	$1. 9 \cdot 10^{08}$	[37]
R9	$8 \cdot 10^{07}$	$2.51 \cdot 10^{08}$	[36]
R10	$2.24 \cdot 10^{12}$	$1.67 \cdot 10^{08}$	[34]
R11	$2.12 \cdot 10^{11}$	$2.05 \cdot 10^{08}$	[34]
R12	$9.87 \cdot 10^{08}$	$3.1 \cdot 10^{07}$	[34]

The NO_x generation and reduction model

The NO_x emitted into the atmosphere from pulverized coal at atmospheric pressure consists mainly of NO (more than 90%), which originates from airborne N_2 and fuel N (thermal NO and fuel NO) [38, 39]. The formation of thermal NO is based on the extended Zeldovich mechanism. Fuel nitrogen is specified as volatile nitrogen and char nitrogen after the completion of devolatilization. Assuming that fuel NO from volatile nitrogen is formed through the transient evolution of hydrogen cyanide (HCN). The small evolution of ammonia (NH_3) is ignored. Fuel NO is based on De Soete's proposed global reaction mechanism. For the heterogeneous reduction of NO by char, the model derived by Levy is used to describe the reaction rate of NO reduction.

Considering the property that CH_4, CO, and H_2 can reduce NO in homogeneous phase [35, 40, 41], the reburning model is used to describe the NO reduction process. The reduction efficiency is related to the local equivalence ratio, temperature, component concentration and mixing rate. In the temperature interval of 1600-2100 K, NO reacts with unburned hydrocarbons, leading to the decrease of NO concentration.

The NO mass concentration:

$$\rho\left(\mathrm{NO}_x\right) = \frac{\varphi(\mathrm{NO})}{0.95} 2.05 \frac{21-6}{21-\varphi\left(\mathrm{O}_2\right)} \tag{9}$$

where $\rho(\mathrm{NO}_x)$ [mgm^{-3}] is the mass concentration of NO_x in dry flue gas with 6% oxygen at standard conditions, φ(NO) [10^{-6}] – the volume fraction of NO in dry flue gas, and $\varphi(\mathrm{O}_2)$ – the volume fraction of oxygen in dry flue gas.

Results and discussion

Mesh independent validation and CFD result validation

The 725680, 1050924, and 1290756 hexahedra cells are used for grid independent validation. The O_2 and temperature distributions along the centerline of the burner are taken in each set of grids, as shown in figs. 3(a) and 3(b). The calculation results with 725680 cells deviate significantly from those of the other two sets of grids, while the calculation results for cells 1050924 and 1290756 are similar. Considering the calculation cost and accuracy, the mesh with 1050924 cells is used for all subsequent calculations.

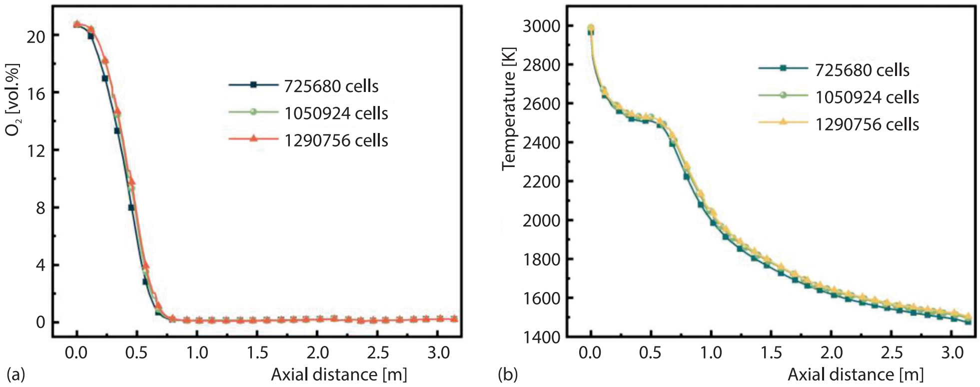

Figure 3. Temperature distribution (a) and O_2 distribution (b) along the burner centerline

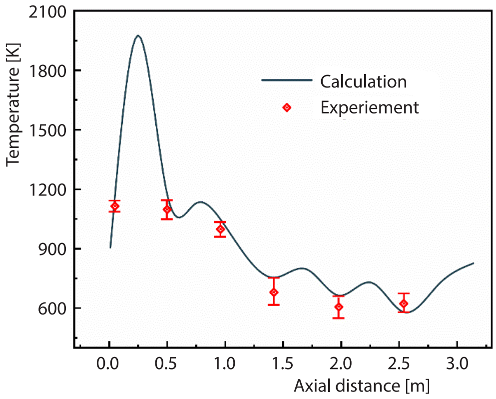

Figure 4. Experimental and simulated temperature validation

A full-scale thermal experiment of the internal combustion burner is conducted on a 660 MW unit with a load of 10 ton per hour. The experimental operating conditions are basically the same as the set boundary conditions. Six platinum-rhodium thermocouples are used to measure the temperature distribution along the burner. The simulation results of the measured point temperatures are compared with the thermocouple measurement results as shown in fig. 4. The maximum deviation between the experimentally measured temperature and the numerically calculated result is 64 K with an error range of ±8.5%, which satisfies the industrial requirements. Therefore, it can be considered that the model selected in this study can predict the actual combustion situation in burner accurately.

Temperature and velocity distribution

Preheating temperature is an important parameter to evaluate the preheating degree of pulverized coal. In this study, a plasma torch is used as the initial heat source to ignite the pulverized coal. The preheating temperature is adjusted by controlling the air coefficient. Figure 5(a) shows the temperature distribution contours of the burner cross-section. The high temperature region shrinks gradually as the air coefficient decreases. In fig. 6, the average temperature of the outlet decreases with the decrease of air coefficient. When the air coefficient is reduced to 0.29, the average temperature of the outlet is 826 K. Zhu *et al.* [5] found that there is an optimal value of the effect of preheating temperature on the nitrogen reduction effect by preheating pulverized coal in circulating fluidized bed. This phenomenon will be discussed in section *The* NO_x *distribution and char conversion analysis.*

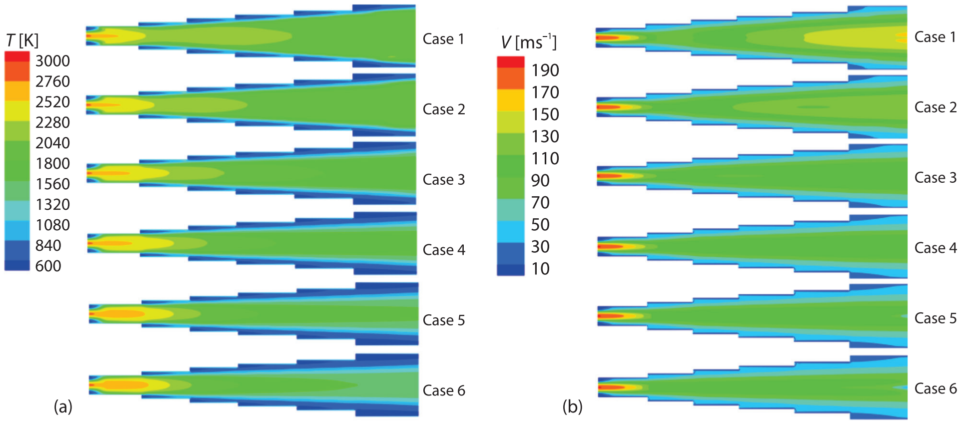

Figure 5. Temperature distribution (a) and velocity distribution (b) of the burner at different loads

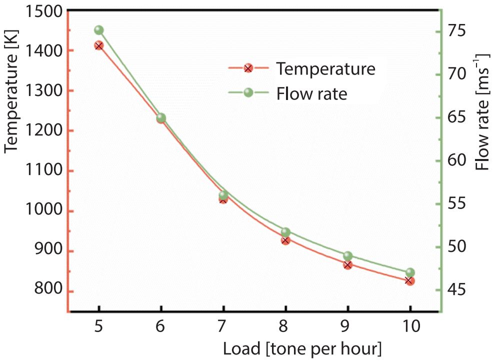

Figure 6. Average temperature and average flow rate of the burner outlet

The burner flow field distribution will directly determine the boiler operation condition, which is an important index to evaluate the burner performance. The accurate simulation of the flow field distribution is the basis for reasonable prediction of the component distribution. The design structure has an important influence on the flow field distribution. Figure 5(b) shows the contours of the velocity distribution of the burner. The average flow rate of the outlet decreases continuously as the air coefficient decreases combined with fig. 6. The trend of the average flow rate of the outlet and the trend of the average temperature of the outlet are basically the same. This is because as the air coefficient decreases, the combustion becomes insufficient resulting in lower temperature and the molecular heat absorption of the gas mixture decreases resulting in lower flow rate.

Gas phase component distribution

The actual operating experience of power plants shows that pulverized coal will precipitate reducing gas by heating and form a local reduction zone under low air coefficient conditions. It can effectively reduce NO_x and lower NO_x emission, such as air stage technology. Coal preheating technology can be regarded as further air stage. In this technology, accurate prediction of reducing gas concentration is a prerequisite for NO_x prediction. The gas phase distribution is shown in fig. 7. It can be found that O_2 is rapidly consumed at the burner inlet, after O_2 is replenished step by step. This structure can continuously provide sufficient heat for pulverized coal preheating and make the volatile matter precipitate rapidly. As can be seen from

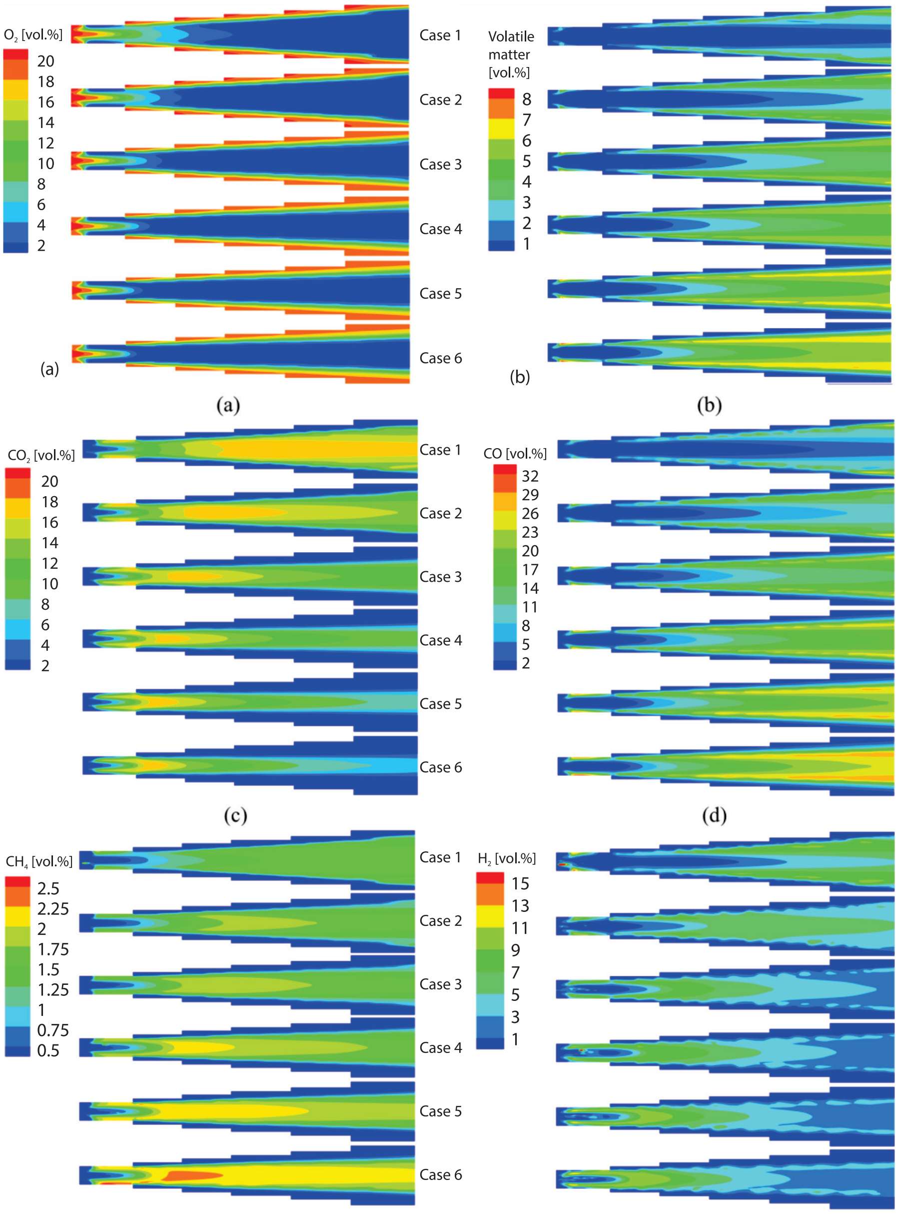

(a) (b) (c) (d)

Figure 7. The O_2 (a), volatile matter (b), CO_2 (c), CO (d), CH_4 (e), and H_2 (f) distribution of the burner at different loads

the change of O_2 volume fraction of the burner outlet in tab. 4, while the air coefficient keeps decreasing, combustion becomes insufficient and the volume fraction of O_2 at the burner outlet increases. Combined with fig. 7(b) and tab. 4, there is obviously volatile matter precipitated and the maximum local concentration reaches 8.3 vol.%.

From figs. 7(c) and 7(d), there is an obvious decreasing trend of CO_2 volume fraction along the burner. While the change trend of CO is exactly the opposite. The volume fraction

Table 4. Gas volume fraction of the burner outlet at different loads [%]

	O_2	Volatile matter	CO_2	CO	CH_4	H_2
Case 1	7.81	2.17	7.09	8.04	0.87	4.54
Case 2	9.79	2.66	4.70	8.69	0.63	2. 33
Case 3	11.92	2.64	2.44	8.95	0.5	1.68
Case 4	12.77	2.66	1.5	9.11	0.51	0.96
Case 5	13.22	2.69	0.94	9.28	0.55	0.81
Case 6	13.49	2.72	0.58	9.4	0.61	0.74

of CO along the burner becomes obviously larger, probably because CO_2 gasification reaction (R4) and water gasification reaction (R8) dominate CO_2 consumption generate CO. The lower the air coefficient, the more obvious such phenomenon is. It can be seen from tab. 4 that when the air coefficient in burner is 0.29, the volume fraction of CO_2 at the burner outlet is only 0.58% and the volume fraction of CO is as high as 9.4%.

The contours of CH_4 distribution in burner are shown in fig. 7(e). The CH_4 can be stably generated in burner with a local maximum concentration up to 2.54 vol.%. Glarborg *et al.* [42] considers CH_4 as an efficient reducing agent. The CH_4 volume fraction decreases along the burner. It is possible that the CH_4 reforming reaction (R9) consumes part of CH_4. In Case 3 the minimum value of CH_4 volume fraction of the burner outlet appears to be 0.5%. When the air coefficient is lower than 0.43, the CH_4 content increases due to the gasification reaction between char and H_2 (R5), which becomes the main influencing factor of CH_4 concentration change. When the air coefficient is higher than 0.43, the increase of O_2 makes the combustion become violent. More volatile matter is analyzed and the volatile matter pyrolysis reaction (R6) leads to the increase of CH_4 volume fraction. Figure 7(f) shows the contours of H_2 distribution in burner. The volume fraction of H_2 decreases along the burner. The gasification reaction between char and H_2 (R5) and water gas reforming reaction (R8) are the main reasons for the consumption of H_2, while CO and CH_4 are produced. As the air coefficient decreases leading to the lower preheating temperature, the volatile matter pyrolysis reaction (R6) is less active and the H_2 volume fraction of the burner decreases according to Arrhenius.

The NO_x distribution and char conversion analysis

The NO distribution contours of the burner outlet are shown in fig. 8. The pulverized coal preheating technology has obvious nitrogen reduction effect. Under the reduction of CH_4, CO, and H_2, the concentration of NO at the burner outlet is maintained low. The locations of NO generation are mainly concentrated in the circular Region I and in the annular Region II. The NO in Region I decreases gradually with the decrease of air coefficient. It may be the thermal NO reduction due to the lower flame temperature. Region II is at the intersection of reducing and oxidizing atmospheres. The fuel nitrogen is oxidized in the annular region form fuel NO.

When the air coefficient in burner is 0.33 and the char conversion rate is 25.58%, the concentration of NO at the burner outlet is only 2.8 mg/Nm^3 from fig. 9. When the air coefficient inside the burner is higher than 0.33, the temperature inside the burner increases with more char oxidation and combustion, which may lead to collapse of char pore structure [5]. This reduces the specific surface area of the coke and leads to lower reducibility. When the air coefficient inside the burner is lower than 0.33, the NO concentration rises to 18.48 mg/Nm^3 at the burner outlet. The reduction efficiency decreases. The reduction effect is influenced by the ambient temperature. As the air coefficient decreases, the burner outlet temperature decreases and the NO reduction reaction activity decreases.

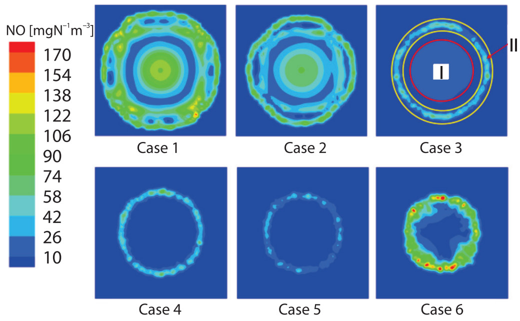

Figure 8. The NO distribution of the burner outlet at different loads

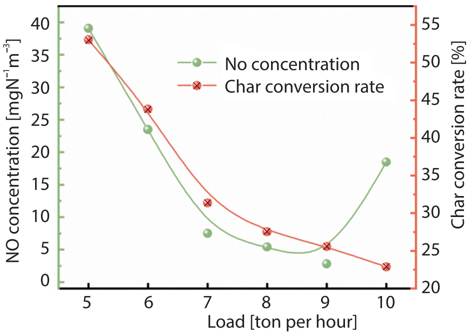

Figure 9. The NO concentration and char conversion rate of the burner outlet at different loads

Conclusions

In this study, the effects of air coefficient on temperature field, velocity field, gas component distribution and NO_x emission of the preheating process are studied experimentally and simulated. The main findings are as follows.

- Numerical simulation coupled with pulverized coal gasification mechanism can successfully predict the reduction products and NO_x during preheating process.
- With the increase of load, the average temperature and velocity of the burner outlet decreases. At an air coefficient of 0.29, the average temperature and average flow velocity of the burner outlet are 826 K and 47.02 m/s, respectively.
- Under the condition of low air coefficient, the burner can produce CH_4, CO, H_2 stably. With the decrease of air coefficient, the effect of CO_2 gasification reaction is obvious. The volume fraction of CO at the burner outlet is up to 9.4%. The maximum local concentration of CH_4 is 2.54 vol.% and the volume fraction of H_2 decreases with the decrease of air coefficient.
- The nitrogen reduction effect of internal combustion burner is remarkable under the condition of low air coefficient. The concentration of NO at the outlet of the combustion burner is maintained low. When the air coefficient is 0.33, the average temperature of the burner outlet is 866 K and the char conversion rate is 25.58%. The burner has the best preheating effect with NO concentration of 2.8 mg/Nm^3 (at 6% O_2) at outlet.

Acknowledgment

The present work was supported by the National Key Research and Development Plan of China (No. 2018YFB0604203).

References

[1] Lv, Z., *et al.*, Experimental Investigation on NO Emission of Semi-Coke under High Temperature Preheating Combustion Technology, *Fuel*, 283. (2021), 119293

[2] Liu, X., *et al.*, Mechanism Study of Nitric Oxide Reduction by Light Gases from Typical Chinese Coals, *Journal of the Energy Institute*, *93* (2020), 4, pp. 1697-1704

[3] Ouyang, Z., *et al.*, The Effect of Limestone on SO_2 and NO_x Emissions of Pulverized Coal Combustion Preheated by Circulating Fluidized Bed, *Fuel*, *120* (2014), Mar., pp. 116-121

[4] Rabovitser, J., *et al.*, Development and Testing of a Novel Coal Preheating Technology for NO_x Reduction from Pulverized Coal-Fired Boilers, *Gas*, *1* (2003), 2, 4

[5] Zhu, J., *et al.*, An Experimental Study on NO_x Emissions in Combustion of Pulverized Coal Preheated in a Circulating Fluidized Bed, *Energy and Fuels*, *27* (2013), 12, pp. 7724-7729

[6] Ren, Q., Bao, S., Combustion Characteristics of Ultrafine Gasified Semi-Char in Circulating Fluidized Bed, *The Canadian Journal of Chemical Engineering*, *94* (2016), 9, pp. 1676-1682

[7] Yao, Y., *et al.*, Experimental Study on Nitrogen Transformation in Combustion of Pulverized Semi-Coke Preheated in a Circulating Fluidized Bed, *Energy and Fuels*, *29* (2015), 6, pp. 3985-3991

[8] Choi, C. R., Kim, C. N., Numerical Investigation on the Flow, Combustion and NO_x Emission Characteristics in a 500 MWE Tangentially Fired Pulverized-Coal Boiler, *Fuel*, *88* (2009), 9, pp. 1720-1731

[9] Zhou, H., *et al*., Numerical Simulation of The NO_x Emissions in a 1000 MW Tangentially Fired Pulverized-Coal Boiler: Influence of the Multi-Group Arrangement of the Separated over Fire Air, *Energy and Fuels*, *25* (2011), 5, pp. 2004-2012

[10] Liu, H., *et al*., Effect of Two-Level over-Fire Air on the Combustion and NO_x Emission Characteristics in A 600 MW Wall-Fired Boiler, Numerical Heat Transfer – Part A: *Applications*, *68* (2015), 9, pp. 993-1009

[11] Kuang, M., *et al*., Numerical Investigation on Combustion and NO_x Emissions of a Down-Fired 350 MWE Utility Boiler with Multiple Injection and Multiple Staging: Effect of the Air Stoichiometric Ratio in the Primary Combustion Zone, *Fuel Processing Technology*, *109* (2013), May, pp. 32-42

[12] Hecht, E. S., *et al*., Effect of CO_2 Gasification Reaction on Oxy-Combustion of Pulverized Coal Char, *Proceedings of the Combustion Institute*, *33* (2011), 2, pp. 1699-1706

[13] Kim, D., *et al*., Effect of CO_2 Gasification Reaction on Char Particle Combustion in Oxy-Fuel Conditions, *Fuel*, *120* (2014), Mar., pp. 130-140

[14] Niu, Y., Shaddix, C. R., A Sophisticated Model to Predict Ash Inhibition during Combustion of Pulverized Char Particles, *Proceedings of the Combustion Institute*, *35* (2015), 1, pp. 561-569

[15] Kajitani, S., *et al*., The CO_2 Gasification Rate Analysis of Coal Char in Entrained Flow Coal Gasifier, *Fuel*, *85* (2006), 2, pp. 163-169

[16] Guo, X., *et al*., Performance of an Entrained-Flow Gasification Technology of Pulverized Coal in Pilot-Scale Plant, *Fuel Processing Technology*, *88* (2007), 5, pp. 451-459

[17] Watanabe, H., Otaka, M., Numerical Simulation of Coal Gasification in Entrained Flow Coal Gasifier, *Fuel*, *85* (2006), 12-13, pp. 1935-1943

[18] Mahmud, T., Sangha, S., Prediction of a Turbulent Non-Premixed Natural Gas Flame in a Semi-Industrial Scale Furnace Using a Radiative Flamelet Combustion Model, *Flow, Turbulence, and Combustion*, *84* (2010), 1, pp. 1-23

[19] Mujumdar, K.S., *et al.*, Modelling of Rotary Cement Kilns: Applications to Reduction in Energy Consumption, *Industrial and Engineering Chemistry Research*, *45* (2006), 7, pp. 2315-2330

[20] Chen, L., *et al*., Oxy-Fuel Combustion of Pulverized Coal: Characterization, Fundamentals, Stabilization and CFD Modelling, *Progress in Energy and Combustion Science*, *38* (2012), 2, pp. 156-214

[21] Chen, M., *et al*., Analysis of Flow Structure of Tunnel Fire Based on Modal Decomposition, *Thermal Science*, *26* (2022), 6B, pp. 5027-5041

[22] Andersen, J., *et al*., Global Combustion Mechanisms for Use in CFD Modelling under Oxy-Fuel Conditions, *Energy and Fuels*, *23* (2009), 3, pp. 1379-1389

[23] Modlinski, N., Computational Modelling of a Utility Boiler Tangentially-Fired Furnace Retrofitted with Swirl Burners, *Fuel Processing Technology*, *91* (2010), 11, pp. 1601-1608

[24] Toporov, D., *et al*., Detailed Investigation of a Pulverized Fuel Swirl Flame in CO_2/O_2 Atmosphere, *Combustion and Flame*, *155* (2008), 4, pp. 605-618

[25] Nikolopoulos, N., *et al*., Numerical Investigation of the Oxy-Fuel Combustion in Large-Scale Boilers Adopting the Eco-Scrub Technology, *Fuel*, *90* (2011), 1, pp. 198-214

[26] Fan, H., *et al*., Numerical Simulation on Heating Performance and Emission Characteristics of a New Multi-Stage Dispersed Burner for Gas-Fired Radiant Tubes, *Thermal Science*, *26* (2021), 5A, pp. 3787-3801

[27] Diez, L. I., *et al*., Numerical Investigation of NO_x Emissions from a Tangentially-Fired Utility Boiler under Conventional and Overfire Air Operation, *Fuel*, *87* (2008), 7, pp. 1259-1269

[28] Yin, C., *et al*., Investigation of the Flow, Combustion, Heat Transfer and Emissions from a 609 MW Utility Tangentially Fired Pulverized-Coal Boiler, *Fuel*, *81* (2002), 8, pp. 997-1006

[29] Modest, M. F., Mazumder, S., *Radiative Heat Transfer*, Academic Press, Cambridge, Mass., USA, 2021

[30] Kobayashi, H., *et al*. Coal Devolatilization at High Temperatures, *Symposium (International) on Com*bus*tion*, *16* (1977), 1, pp. 411-425

[31] Asotani, T., *et al*., Prediction of Ignition Behavior in a Tangentially Fired Pulverized Coal Boiler Using CFD, *Fuel*, *87* (2008), 4-5, pp. 482-490

[32] Adamczyk, W. P., *et al.*, Application of the Computational Method for Predicting NO_x Reduction Within large-Scale Coal-Fired Boiler, *Applied Thermal Engineering*, *73* (2014), 1, pp. 343-350

[33] Das, T., Evolution Characteristics of Gases During Pyrolysis of Maceral Concentrates of Russian Coking Coals, *Fuel*, *80* (2001), 4, pp. 489-500

[34] Ibrahimoglu, B., Yilmazoglu, M. Z., Numerical Modelling of a Downdraft Plasma Coal Gasifier with Plasma Reactions, *International Journal of Hydrogen Energy*, *45* (2020), 5, pp. 3532-3548
[35] Chen, D., *et al*., Optimizing in-Situ Char Gasification Kinetics in Reduction Zone of Pulverized Coal Air-Staged Combustion, *Combustion and Flame*, *194* (2018), Aug., pp. 52-71
[36] Ma, J., Zitney, S. E., Computational Fluid Dynamic Modelling of Entrained-Flow Gasifiers with Improved Physical and Chemical Submodels, *Energy and Fuels*, *26* (2012), 12, pp. 7195-7219
[37] Bustamante, F., *et al.*, Uncatalyzed and Wall-Catalyzed Forward Water-Gas Shift Reaction Kinetics, *AIChE Journal*, *51* (2005), 5, pp. 1440-1454
[38] Edge, P., *et al.*, Combustion Modelling Opportunities and Challenges for Oxy-Coal Carbon Capture Technology, *Chemical Engineering Research and Design*, *89* (2011), 9, pp. 1470-1493
[39] Muto, M., *et al*., Large Eddy Simulation of Pulverized Coal Combustion in Multi-Burner System-Effect of in-Furnace Blending Method in NO Emission, *Advanced Powder Technology*, *30* (2019), 12, pp. 3153-3162
[40] ur Rahman, Z., *et al*., Numerical Assessment of NO_x Evolution in Ammonia Oxidation and Its Control by Reburning in Pressurized Oxy-Combustion, *Journal of the Energy Institute*, *100* (2022), Feb., pp. 89-98
[41] Li, D., *et al.*, Experimental Study and CFD Modelling of NO_x Reduction and Reductive Gas Formation in Deep Reburning of Cement Precalciner, *Fuel Processing Technology*, *229* (2022), 107183
[42] Glarborg, P., *et al*., Modelling Nitrogen Chemistry in Combustion, *Progress in Energy and Combustion Science*, *67* (2018), pp. 31-68

Paper submitted: September 19, 2022
Paper revised: December 10, 2022
Paper accepted: December 18, 2022